# Protein adsorption materials of the soluble conducting polymer poly(acryloyl chloride)-g-polypyrrole

Zhihong Zhang,*[ab] Yan Liang,[a] Lijun Yan,[a] Fufeng Yan[a] and Shaoming Fang*[a]

*Received (in Gainesville, FL, USA) 8th January 2010, Accepted 11th June 2010*
**DOI: 10.1039/c0nj00013b**

In order to fabricate a soluble conducting polypyrrole matrix, applied as a biomaterial to anchor proteins, the preparation of a poly(acryoyl pyrrole)-g-polypyrrole (PAP-g-PPy) copolymer and the adsorption of bovine serum albumin (BSA) onto this conducting copolymer were studied. Polypyrrole (PPy) was synthesized by electrochemical polymerization on an Au surface, which had been spin-coated with a poly(acryloyl chloride) precursor containing a pyrrole moiety in its side chain. The chemical properties of PPy depend on the polymerization conditions, *i.e.*, the concentration of pyrrole and the polymerization time. Subsequently, the adsorption behavior of BSA on PAP-g-PPy was investigated by surface plasmon resonance spectroscopy, suggesting that the copolymer thickness, the concentration of pyrrole monomer used in the preparation of the polymer, the BSA concentration and the pH value of buffer solutions can affect the adsorption behavior of BSA onto the polymer surface. It is therefore predicted that the conducting copolymer PAP-g-PPy could be used as an adsorbed matrix for protein adsorption.



## 1. Introduction

Recently, polypyrrole (PPy) has been proved to be an important conductive polymer due to its unique properties, *i.e.*, high environmental stability, good redox properties, high electrical conductivities and biocompatibility.[1–3] Also, PPy can be easily prepared *via* chemical[4,5] or electrochemical methods,[6,7] and doped with various anions.[8,9] As a promising type of biomaterial, conducting PPy has been applied as the matrix for PNA or DNA immobilization/hybridization,[10] cell adhesion[11,12], drug delivery[13] and detection,[14] protein adsorption, *etc*. Protein adsorption onto PPy surfaces is very actively studied for the development of biomaterials, biological assays and biosensors, in addition to the fundamental research on its driving mechanisms. For example, an array of spotted proteins has been fabricated by the copolymerization of pyrrole/pyrrole–protein using surface plasmon resonance (SPR) imaging, monitoring being ensured by a CCD camera.[15] Human serum albumin was covalently adsorbed onto reactive polypyrrole-coated polystyrene latex particles (PS-PPy) and as a result the PS-PPy particles could be an alternative candidate for visual diagnostic assays.[16]

However, most polypyrrole derivatives exhibit poor environmental stability, solubility, brittleness and poor processibility. Moreover, the interaction between biomolecules and a pristine PPy surface has been shown to be weak. Normally, pyrrole derivatives (with some functional groups or other molecules, such as amino, carboxy acid and biomolecules) are used and copolymerized with pyrrole monomer. Although Park *et al.*[17] have reported the synthesis of a soluble conducting graft copolymer of poly(acryoyl pyrrole) (PAP) and polypyrrole, PAP-g-PPy, by using a precursor polymer (PAP), no further work was done on biomolecule adsorption onto PAP-g-PPy surfaces. To understand the adsorption behavior of protein molecules onto surfaces of this kind of soluble conducting polymer, the authors fabricated the PAP-g-PPy copolymer on Au surfaces and investigated the immobilization of bovine serum albumin (BSA) on the surfaces by SPR in detail.

## 2. Experimental section

### 2.1 Materials and regents

BSA was purchased from Shanghai Biolife Science & Technology Co., Ltd., with a molecular weight of 67 000. Acryloyl chloride monomer was purified by distillation in air at 78 °C. The initiator 2,2-azobisisobutyonitrile (AIBN) was purified by recrystallization in methanol using an ice/salt mixture. Pyrrole and acetonitrile were dried by distillation with calcium hydride. Tetrahydrofuran (THF) was distilled with sodium and benzophenone. Dimethylformamide (DMF) was purified by distillation under reduced pressure. Other chemicals were used without further purification.

### 2.2 BSA adsorption onto the surface of PAP-g-PPy

Poly(acryloyl pyrrole) (PAP) was synthesized using a procedure similar to that reported by Park *et al.*[17] Afterwards, a DMF solution of PAP was spin-coated onto an Au film and the precursor polymer was chemically graft-copolymerized in a solution of $1.5 \times 10^{-3}$ mol pyrrole monomer and 1.5 M $FeCl_3$. The PAP-g-PPy film was subsequently thoroughly rinsed with distilled water and atmospherically dried.

[a] *Henan Provincial Key Laboratory of Surface & Interface Science, Zhengzhou University of Light Industry, No. 5 Dong Feng Rd, Zhengzhou, China 450002. E-mail: mainzhh@yahoo.com.cn; Fax: + 86 371 63556510; Tel: +86 371 63556510*
[b] *Departmental of Materials Science and Engineering, Gwangju Institute of Science and Technology, 1 Oryong-dong, Buk-gu, Gwangju, 500-712, South Korea. Fax: +82 629702363; Tel: +82 62 9702363*

 

### 2.3 Preparation of PBS solutions

Solution A: 9.465 g of $Na_2HPO_4{\cdot}12H_2O$ dissolved into 1000 mL de-ionized water.

Solution B: 9.07 g of $KH_2PO_4$ dissolved into 1000 mL de-ionized water.

Solutions A and B were stored at 4 °C in brown bottles. The two solutions were mixed together in different quantities to achieve different pH values of PBS (see Table 1).

### 2.4 Fourier transform infrared spectroscopy (FTIR) spectra of the films

FTIR spectra of pure PPy films were recorded using a Nicolet 5700 FTIR spectrometer (Thermo Electron Corporation) using the KBr pellet method. The spectra were recorded from 4000 to 400 $cm^{-1}$, with a 4 $cm^{-1}$ resolution for 32 scans.

### 2.5 X-Ray photoelectron spectroscopy (XPS) measurement and XPS peak fitting

The XPS measurements were performed on a Kratos AXIS HSi spectrometer using a monochromotized AL K X-ray source (1486.71 eV photons) with a pass energy of 40 eV. Samples were mounted on the sample studs by double-sided adhesive tape. The XPS signals were obtained at a photoelectron take-off angle of 90° (with respect to the sample surface). The X-ray source was run at a power of 150 W (15 kV and 10 mA). The pressure in the analysis chamber was maintained at $10^{-8}$ Torr or lower during each measurement. All binding energies (BEs) were referenced to the C 1s hydrocarbon peak at 284.6 eV. Surface elemental stoichiometries were determined from XPS spectral area ratios after correcting with experimentally-determined sensitivity factors. The peaks in the elemental core-level spectra were fitted using commercial XPS analysis software. The number of peaks chosen for each fit was the minimal number required to obtain random residuals. A linear function was used to model the background, with the corresponding coefficients fitting simultaneously with the peaks.

### 2.6 Cyclic voltammogram (CV) measurements

Cyclic voltammograms were measured with a BAS 100B Electrochemical Analyzer before and after hybridization. Conventional three-electrode cells comprising Pt slides as counterelectrodes and Ag/AgCl (in saturated KCl) as a reference electrode were used. The cyclic voltammograms were obtained in PBS solution under a nitrogen atmosphere.

### 2.7 SPR measurements

A glass slide covered with a gold film prepared for use with the SPR apparatus (SPR 2005, Electronic Institute of Chinese Academy of Sciences, China) was pressed onto the base of a half-cylindrical lens ($n$ = 1.61) *via* an index-matching oil. Linearly p-polarized light having a wavelength of 670 nm from a diode laser was directed through the prism onto the gold film in the Kretshmann configuration. The intensity of the reflected light was measured as a function of the angle of incidence, $\theta$, using a photodiode by a chopper/lock-in amplifier technique. For SPR detection, the as-prepared Au/glass substrates were mounted against the Teflon cuvette of 1 mL volume using a Kalrez O-ring, which provided a liquid-tight seal. The baseline of the SPR binding curve was obtained after injecting a buffer, 0.01 M PBS (pH = 7.4), into the cuvette. In order to investigate the influence of pH, solution buffers of pH 4.9, 5.6, 6.6, 7.4 and 8.0 were used. After obtaining a stable baseline, the protein solution was added to replace the buffer solution. After measuring the binding curve, the solution was changed back to buffer again. All experiments were conducted at room temperature.

The de Feijter formula (eqn (1))[18] was used to quantify the adsorbed mass $\Gamma$ (mg $m^{-2}$) from the film thickness ($d_f$, expressed in nm), refractive index of the film ($n_f$) and the refractive index of the buffer ($n_{buffer}$):

$$\Gamma = d_f (n_f - n_{buffer})/[dn/dc] \quad (1)$$

A $dn/dc$ value of 0.18 mL $g^{-1}$ was used for the calculations. The SPR instrument expresses the shift in $\theta$ as resonance units (RU). The RU contains a calibration constant that converts shifts in $\theta$ to adsorbed amounts (μg $m^{-2}$). It has been found that 1 RU corresponds to 1 μg $m^{-2}$ for protein molecules.[19,20] The refractive index of BSA used here is 1.45.[21] The refractive index of the buffer solution is in the range 1.33–1.34. Hence, $d_f$ could be calculated by eqn (2), which is derived from eqn (1) if the adsorbed mass of protein is estimated.

$$d_f \approx 1.5\Gamma \text{ nm} \quad (2)$$

**Table 1** The preparation of PBS with different pH values

| pH | 4.9 | 5.6 | 6.6 | 7.4 | 8.0 |
|---|---|---|---|---|---|
| A/mL | 0.1 | 0.5 | 4.0 | 8.0 | 9.5 |
| B/mL | 9.9 | 9.5 | 6.0 | 2.0 | 0.5 |

## 3. Results and discussion

### 3.1 The chemical structure of PAP and PAP-g-PPy characterized by FTIR and XPS

To maintain constant experimental conditions, PAP and PAP-g-PPy were spin-coated and polymerized onto Au surfaces for FTIR measurements, respectively. Fig. 1 shows the FTIR spectra of the PAP and PPy-g-PPy films. PAP shows a characteristic peak at 1725 $cm^{-1}$ due to the C═O bond, which is not present in PAP-g-PPy. However, a substantial peak at 1545 $cm^{-1}$ due to the C═C bond in the heterocycle of pyrrole is observed in PPy-g-PPy films.

Fig. 2 shows the XPS spectra of C 1s and N 1s of PAP-g-PPy film, which was obtained after the pyrrole was polymerized for 4 min. The C 1s core-level spectra of PAP-g-PPy can be decomposed into three components. The peaks of C–H and C–N are centered at a binding energy of 284.6 eV. The peaks at 286.3 and 288 eV can be assigned to C–O/C–N and C═O groups, respectively. Since the oxidation potential of PPy is lower than that of pyrrole monomer, the polymer could be oxidized easily with pyrrole during the process of the polymerization reaction.[22] As shown in Fig. 3, the N 1s core-level spectra of PAP-g-PPy can be fitted into four peaks. Binding energies of 396.0 and 399.4 eV are due to the imine (–N═) and amine (–NH–) bonds, respectively. The higher binding

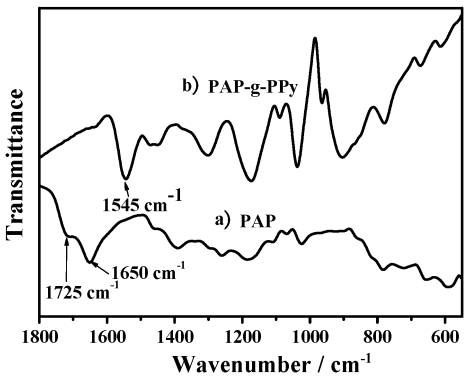


**Fig. 1** Comparison of the FTIR spectra of (a) PAP and (b) PAP-g-PPy.

energies of 399.5 and 401 eV can be assigned to two higher oxidation states of the nitrogen atoms or protonated nitrogen atoms with positive charges. The positively charged nitrogen atoms, which play an important role in the adsorption of BSA onto PAP-g-PPy, were approximately 9.6% (*i.e.*, $[N^+]/[N]$).

### 3.2 The electrochemical properties of PAP-g-PPy before and after protein adsorption

Fig. 3 shows the cyclic voltammograms obtained for the PAP-g-PPy copolymer after 5 min polymerization at scan rates of 80, 120 and 140 mV $s^{-1}$ before and after BSA adsorption. The thickness of PAP-g-PPy used is approximately 110 nm, which was detected by ellipsometry. The CV curves for the PAP-g-PPy copolymer have an apparent reduction peak, while there is no clear oxidation peak. This indicates that the copolymer exhibits high electroactivity in buffer solutions. After the BSA anchor, however, the chemical content of the copolymer with BSA in the composite electrodes changes, which results in an electroactivity decrease of the copolymer with BSA. At the same scan rate, 120 mV $s^{-1}$, the cathode peak potential of the copolymer is 420 mV and the approximate separation between the oxidation and reduction peak is about 710 mV. After BSA adsorption, the cathode peak potential shifts to 360 mV, while the separation decreases to 630 mV. The result could be explained by the full covering of BSA on the copolymer surface. Hence, the huge conjugated part in the copolymer could not exhibit a strong electroactivity.

### 3.3 The adsorption behavior of BSA on the PAP-g-PPy surfaces

**(i) The effect of the polymerization time of PAP-g-PPy on the adsorption of BSA.** The kinetic curves of BSA adsorption behavior onto PAP-g-PPy films prepared for 1, 2, 3 and 4 min are summarized in Fig. 4(a). For all the samples studied, protein physisorption reached equilibrium within a few minutes after injecting the protein into the cell. The systems were allowed to stabilize over a period of 1 h but showed no further significant changes. After this stabilization period, the samples were rinsed with PBS, which, in all cases of the PAP-g-PPy films, always caused a loss of some unbound protein from the surface.

Different adsorption behavior was observed on PAP-g-PPy films of 15, 21, 35 and 48 nm thickness under varying polymerization times of 1, 2, 3 and 4 min. A larger adsorbed amount of BSA on polymer films was observed, even for the polymerization time of 4 min. Since the structure of BSA is a globular protein with dimensions of approximately 8 nm by 4 nm. This suggests that the thickness of BSA molecules will be 4 nm if BSA adsorbs onto the surfaces in a side-on orientation. As the polymerization time was increased, *i.e.* with increasing polymer thickness, fewer BSA molecules remained after rinsing with PBS buffer. Only less than a monolayer of BSA could be adsorbed on the surface of PAP-g-PPy under the polymerization times of 3 and 4 min. In fact, once the polymerization had started between the pyrrole groups of PAP-g-PPy and the added pyrrole monomer, the first propagation of the polymerization only focused on certain points on the surface. The PAP-g-PPy did not uniformly distribute on the PAP surface and thus it was not fully covered. PPy molecules have enough space to stretch and more BSA molecules will interact with polymer surface. BSA molecules not only adsorbed on the polymerized surface, but also onto the PAP surface. At the thinnest places of the surface, far more BSA molecules are able to lie onto the polymer surface one by one to form a monolayer. This resulted in more protein molecules remaining on the surface. As the polymerization time was increased, the whole surface became fully covered by PPy, which led to a much denser PPy surface. The steric hindrance of pyrrole becomes much bigger, resulting in less interaction between BSA and the surface. Consequently, less BSA was adsorbed onto this kind of surface.

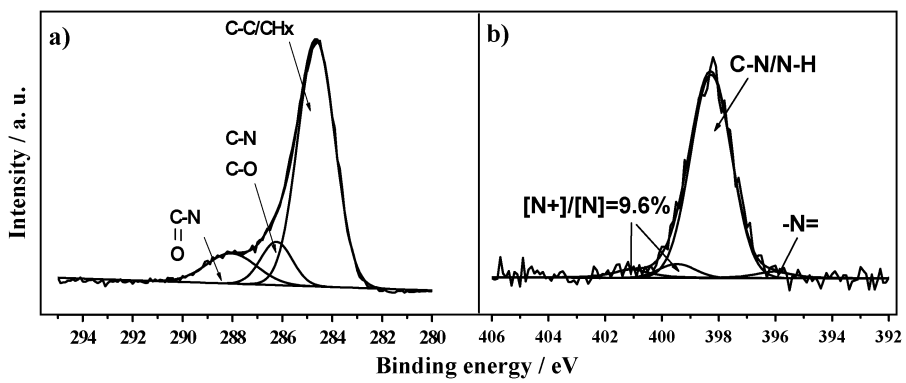


**Fig. 2** The XPS spectra of (a) C 1s and (b) N 1s core-level of PAP-g-PPy films prepared for 4 min with the thickness of 20 nm.

 

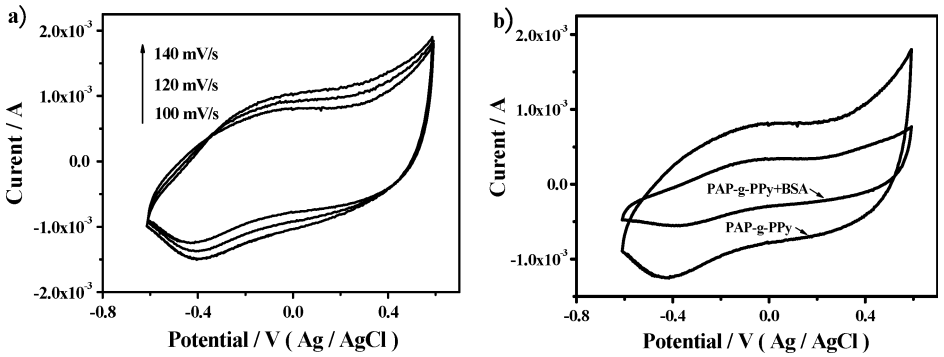


**Fig. 3** Cyclic voltammetry graphs of PAP-g-PPy (a) before and (b) after BSA adsorption. The scan rates of (a) are 100, 120 and 140 mV $s^{-1}$, while that of (b) is 120 mV $s^{-1}$.

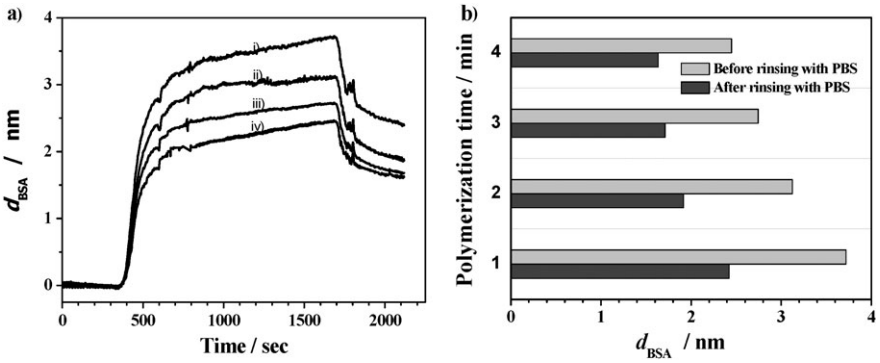


**Fig. 4** Effect of the thickness of PAP-g-PPy on BSA adsorption: (a) SPR binding curves of the adsorption of BSA on PAP-g-PPy films of (i) 15, (ii) 21, (iii) 35 and (iv) 48 nm prepared for 1, 2, 3 and 4 min, and (b) the adsorbed amount of BSA on PAP before and after rinsing with PBS.



**(ii) The effect of the pH of buffer solutions on BSA adsorption.** When 1% BSA was adsorbed onto the PAP-g-PPy surfaces in buffer solutions of various pH values, different amounts were adsorbed, as shown in Fig. 5. After being rinsed with PBS, more BSA molecules remained on the PAP-g-PPy films in buffer solutions with lower pH values. Actually, BSA molecules are negatively-charged in buffer solutions with pH $>$ 4.7 and positively-charged in buffer solutions with a pH $<$ 4.7. The positively-charged PPy film repels BSA molecules in buffers with pH $<$ 4.7 but attracts BSA molecules in buffers with pH $>$ 4.7. This would suggest that the lower the buffer pH value, the more adsorbed BSA molecules remain on the PPy film. Furthermore, almost a 4 nm monolayer of BSA could remain on the polymer surface in a side-on orientation in PBS at pH 4.7. However, BSA molecules with an average thickness of 1.3 nm could be adsorbed onto in PBS at pH 8.0.

**(iii) The effect of BSA concentration on BSA adsorption.** The kinetic behavior of BSA adsorbed onto a 20 nm PAP-g-PPy film is shown in Fig. 6. For BSA of low concentration, this process takes longer compared to BSA of higher concentrations. For example, it took 40 min for 0.1% BSA adsorbed onto PAP-g-PPy films to reach a constant value. However, in the case of 2% BSA, it only took 1000 s. The higher the

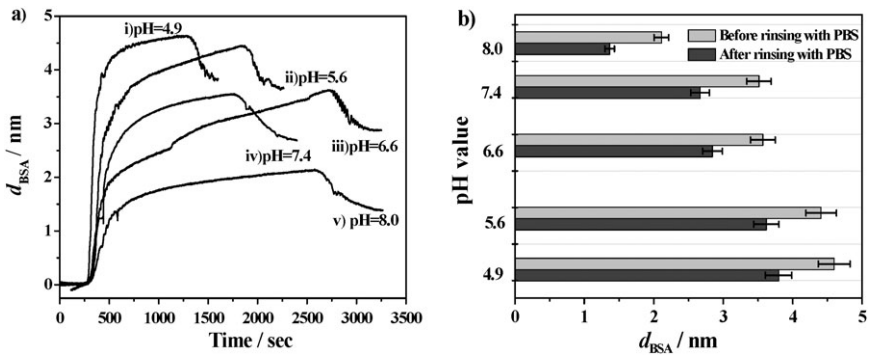


**Fig. 5** Effect of the pH value of the buffer solution on BSA (1%) adsorption on PAP-g-PPy: (a) SPR binding curves of the adsorption of BSA on PAP-g-PPy films in buffer solutions with a pH of (i) 4.9, (ii) 5.6, (iii) 6.6, (iv) 7.4 and (v) 8.0, and (b) the adsorbed amount of BSA on PAP before and after rinsing with PBS.

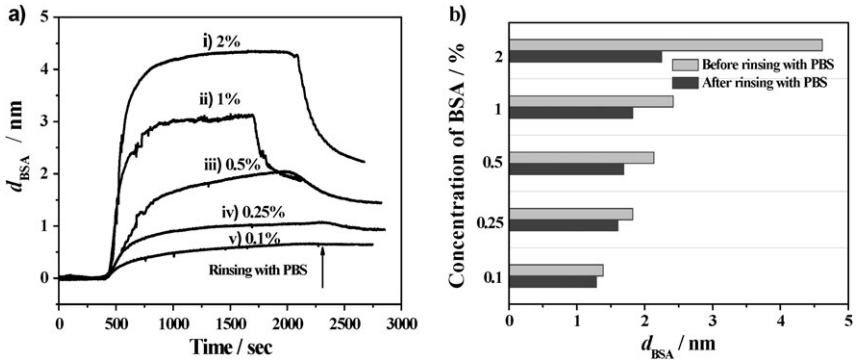


**Fig. 6** (a) SPR binding curves of the adsorption of (i) 2%, (ii) 1%, (iii) 0.5%, (iv) 0.25% and (v) 0.1% BSA on PAP-g-PPy films, and (b) the adsorbed amount of BSA on PAP before and after rinsing with PBS.

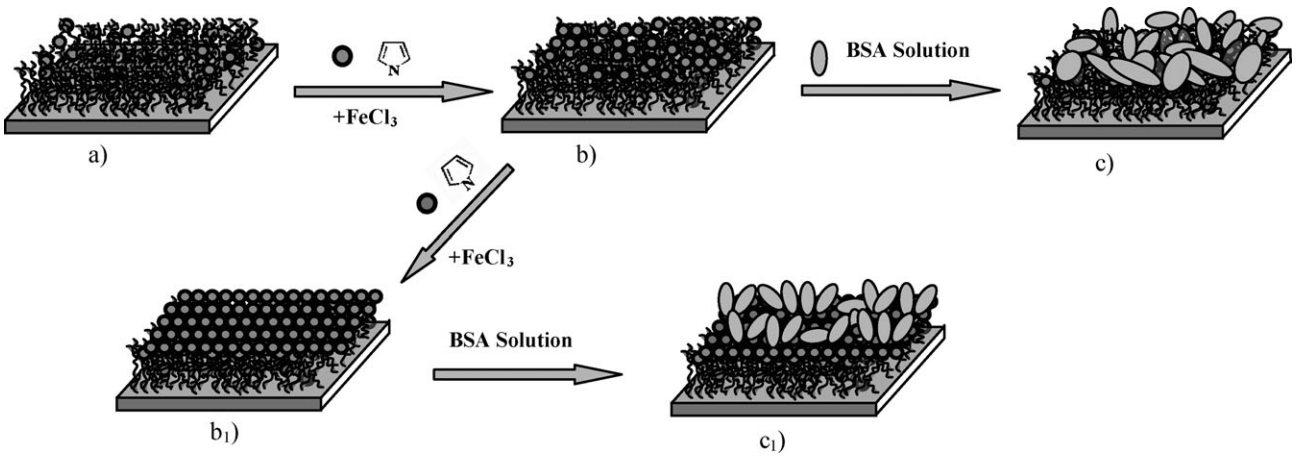


**Fig. 7** BSA adsorption on thin and thick PAP-g-PPy films prepared under different times. It includes the steps of (a) PAP film, (b) thin PAP-g-PPy film, (c) BSA molecule adsorption on thin a PAP-g-PPy film, ($b_1$) a thick PAP-g-PPy film and ($c_1$) BSA molecule adsorption on a thick PAP-g-PPy film.



concentration of BSA, the shorter time it takes to reach the maximum adsorption amount. Once adsorption had reached the equilibrium value, protein molecules adsorbed by physical interactions were removed by rinsing with a large amount of PBS solution. Since there is the linear relationship between the amount of BSA adsorbed and the reflectivity,[23,24] the difference of the reflectivity before and after rinsing with PBS should consequently represent the real amount of BSA adsorbed, as shown in Fig. 6(b).

### 3.4 The adsorption mechanism of BSA on thin and thick PAP-g-PPy films

To aid the following discussion of the adsorption mechanism of BSA on polymer films, the procedure of protein adsorption is shown in Fig. 7. More BSA molecules are able to remain on bare PAP films. Since PAP films were synthesized by radical polymerization, they could swell in the buffer solution and produce a three-dimensional network structure (see Fig. 7(a)). When incubating a BSA solution, the BSA molecules not only adsorb onto the surface of PAP through hydrophobic or electrostatic interactions, but also penetrate into the inner of the polymer. This penetration effect is weaker when the pyrrole molecules polymerize slowly, as shown in Fig. 7(b) and (c). Once the huge conjugation structure of PPy is formed over longer polymerization times (see Fig. $7b_1$), the PPy layer will fully cover the PAP surface, which leads to a much denser layer. Due to this steric effect of PPy films, BSA molecules can only adsorb onto the surface of the PPy layer, resulting in less BSA remaining on the surface (Fig. $7c_1$).

## 4. Conclusions

The soluble conducting copolymer PAP-g-PPy was prepared from a precursor with a pyrrole moiety in its side-chain. The copolymer was characterized in terms of chemical structure and surface wettability. 9.6% $[N^+]/[N]$ was found in the PAP-g-PPy films, which explains the electrostatic interaction between BSA molecules and the polymer in PBS solutions with a pH $>$ 4.7. After BSA adsorption, the electroactivity of the copolymer composite electrodes became weaker because the conjugated copolymer was fully covered by BSA molecules. The PAP-g-PPy film prepared with a polymerization time of 1 min appears to have a higher affinity for BSA. In contrast, less BSA was adsorbed on a thick PAP-g-PPy film. It is difficult to adsorb BSA molecules onto the relatively regular structure of the big conjugation backbone of thick PPy films. As a result of this investigation, it appears that soluble

 

conducting polymers could be attractive biomaterials for protein adsorption.

## Acknowledgements

This work was supported by the Program for the National Natural Science Foundation of China (NSFC: Account no. 20704039).

## References

1 G. Sabouraud, S. Sadki and N. Brodie, *Chem. Soc. Rev*., 2000, **29**, 283.
2 M. D. Shirsat, C. O. Too and G. G. Wallace, *Electroanalysis*, 2008, **20**, 150.
3 A. Ramanavicius, A. Ramanaviciene and A. Malinauskas, *Electrochim. Acta*, 2006, **51**, 6025.
4 R. Akinyeye, I. Michira, M. Sekota, A. A. Ahmed, P. Baker and E. Iwuoha, *Electroanalysis*, 2006, **18**, 2441.
5 Y. Li, W. X. Zhang, G. T. Li and Y. Ju, *Polymer*, 2008, **49**, 225.
6 Y. Wang, G. A. Sotzing and R. A. Weiss, *Chem. Mater*., 2008, **20**, 2574.
7 H. J. Kharat, K. P. Kakde, P. A. Savale, K. Datta, P. Ghosh and M. D. Shirsar, *Polym. Adv. Technol*., 2007, **18**, 397.
8 X. T. Zhang, J. Zhang, W. H. Song and Z. F. Liu, *J. Phys. Chem. B*, 2006, **110**, 1158.
9 P. C. Pandey and G. Singh, *J. Appl. Polym. Sci*., 2008, **107**, 2594.
10 Z. Z. Zhang, P. Liang, X. J. Zheng, D. L. Peng, F. F. Yan, R. Zhao and C. L. Feng, *Biomacromolecules*, 2008, **9**, 1613.
11 D. D. Ateh, H. A. Navsaria and P. Vadgama, *J. R. Soc. Interface*, 2006, **3**, 741.
12 B. Lakard, L. Ploux, K. Anselme, F. Lallemand, S. Lakard, M. Nardin and J. Y. Hihn, *Bioelectrochemistry*, 2009, **75**, 148.
13 R. Okner, Y. Shaulov, N. Tal, G. Favaro, A. J. Domb and D. Mandler, *ACS Appl. Mater. Interfaces*, 2009, **1**, 758.
14 C. C. J. Yu and E. P. C. Lai, *Synth. Met*., 2004, **143**, 253.
15 L. Grosjean, B. Cherif, E. Mercey, A. Roget, Y. Levy, P. N. Marche, M. B. Villiers and T. Livache, *Anal. Biochem*., 2005, **347**, 193.
16 S. Bousalem, S. Benabderrahmane, Y. Y. C. Sang, C. Mangeney and M. M. Chehimi, *J. Mater. Chem*., 2005, **15**, 3109.
17 Y. H. Park, K. W. Kim and W. H. Jo, *Polym. Adv. Technol*., 2002, **13**, 670.
18 J. A. De Feijter, J. Benjamins and F. A. Veer, *Biopolymers*, 1978, **17**, 1759.
19 R. Karlsson and R. Stahlberg, *Anal. Biochem*., 1995, **228**, 274.
20 E. Stenberg, B. Persson, H. Roos and C. Urbaniczky, *J. Colloid Interface Sci*., 1991, **143**, 513.
21 Z. Zhang, B. Menges, R. B. Timmons, W. Knoll and R. Foerch, *Langmuir*, 2003, **19**, 4765.
22 E. D. Giglio, C. D. Calvano, I. Losito, L. Sabbatini, P. G. Zambonin, A. Torrisi and A. Licciardello, *Surf. Interface Anal*., 2005, **37**, 580.
23 D. K. Kambhampati and W. Knoll, *Curr. Opin. Colloid Interface Sci*., 1999, **4**, 273.
24 W. Knoll, *Annu. Rev. Phys.Chem*., 1998, **49**, 569.